show that the compression isotherms can be quantitatively related to the nature of the cation in the subphase and its concentration. At the air-water interface, the polymer is in a highly extended conformation, and cooperative binding between proximate crown ether groups is precluded. Accordingly, the binding characteristics of the polymer at the air-water interface mirrors that of the monomer benzo-18-crown-6 in solution and differs dramatically from that of P18C6 in solution.

Acknowledgment. We thank Ms. Anita VanLaeken of this laboratory for GPC characterization of poly(4'-vinylbenzo-18-crown-6) and Dr. David Tirrell (University of Massachusetts, dept. of Polymer Science and Engineering) for his careful and constructive review of the original manuscript.

Calculation of the Electronic Spectra and Excited-State Distortions of $W(CO)_5$(N-donor) from Preresonance Raman Intensities

Lee Tutt† and Jeffrey I. Zink*

Contribution from the Department of Chemistry, University of California at Los Angeles, Los Angeles, California 90024. *Received March 6, 1985*

Abstract: Excited-state distortions of $W(CO)_5$(pyridine) and $W(CO)_5$(piperidine) are calculated from emission spectra and preresonance Raman spectra by using the time-dependent theory of molecular spectroscopy. The time-dependent theory is described and the connections between electronic spectra and preresonance Raman spectra are discussed. The 10 K emission spectra and the preresonance Raman spectra of the two compounds are reported. Vibronic structure is observed in the spectra of both compounds. The crystal structure and the ground-state bond lengths are reported for $W(CO)_5$(pyridine). The excited-state distortions along 18 normal vibrational modes are calculated by using the combination of electronic spectroscopy, Raman spectroscopy, and time-dependent theory. The emission spectra are calculated from the preresonance Raman-determined intensities. The largest excited-state distortions are those which occur along the molecular axis containing the nitrogen donor ligand. These distortions are associated with the increase in antibonding along this axis caused by increased d_{z^2} σ antibonding in the excited state. In the case of $W(CO)_5$(pyridine), the W-N bond is lengthened by 0.18 Å, and the W-C bond trans to the pyridine is lengthened by 0.12 Å. The cis W-C bonds are only lengthened by 0.04 Å. The connections between the excited-state bond-length distortions and the photochemical reactivity of the molecules are discussed. The vibronic bands in the luminescence spectra of both molecules exhibit a new effect, the "missing mode effect" or MIME effect. Ground-state vibrational frequencies corresponding to the observed regularly spaced vibronic features in the emission spectra are missing. The origin of the MIME effect is explained.

The electronic emission and absorption spectra of large organometallic molecules in condensed media typically contain broad featureless bands. Spectra of these molecules at low temperatures sometimes reveal vibronic structure, but the individual vibronic components are usually not well-resolved. Instrumental resolution in these experiments is usually several orders of magnitude greater than the resolution seen in the spectrum. A typical example, that of the emission and absorption spectra of $W(CO)_5$(pyridine) at 10 K, is shown in Figure 1.

The information contained in the intensities and spacings of vibronic components of electronic spectra is important for understanding the properties of the excited and ground electronic states. Of particular interest in many spectroscopic and photochemical studies are the distortions the molecule undergoes upon electronic excitation.[1] However, detailed determination of excited-state structure via a Franck-Condon analysis, for example, is only possible when highly resolved spectra are available.[2-9]

Detailed calculations of excited-state distortions and structures and an intuitive understanding of the meaning of band widths and poorly resolved vibronic features are obtainable from the newly developed time-dependent theory of molecular spectroscopy.[10-12] In this theory, each vibrational degree of freedom and its displacement are explicitly considered. The theory connects preresonance Raman spectrsocopy, electronic absorption and emission spectroscopy, and geometry changes between the ground and excited electronic states. It has been applied to a limited number of transition metal and organic systems.[13-17]

The purpose of this paper is to combine preresonance Raman spectroscopy, which contains information complementary to electronic spectra, with the absorption and emission spectra to provide a detailed understanding of the excited-state distortions along the multidimensional excited-state potential surface. A new

† Current address: Hughes Research Laboratories, Malibu, CA 90265.

(1) Geoffroy, G. L.; Wrighton, M. S. *Organometallic Photochemistry*; Academic Press: New York, 1979.
(2) Hipps, K. W.; Merrell, G. A.; Crosby, G. A. *J. Phys. Chem.* **1976**, *80*, 2232.
(3) (a) Patterson, H. H.; DeBerry, W. J.; Byrne, J. E.; Hsu, M. T.; LoMenzo, J. A. *Inorg. Chem.* **1977**, *16*, 1698. (b) Patterson, H. H.; Godfrey, J. J.; Kahn, S. M. *Ibid.* **1972**, *11*, 2872.
(4) Urushiyama, A.; Kupka, H.; Degen, J.; Schmidtke, H. *Chem. Phys.* **1982**, *67*, 65.
(5) Wilson, R. B.; Solomon, E. I. *Inorg. Chem.* **1978**, *17*, 1729.
(6) Rice, S. F.; Wilson, R. B.; Solomon, E. I. *Inorg. Chem.* **1980**, *19*, 3425.
(7) Wilson, R. B.; Solomon, E. I. *J. Am. Chem. Soc.* **1980**, *102*, 4085.
(8) Yersin, H.; Otto, H.; Zink, J. I.; Gliemann, G. *J. Am. Chem. Soc.* **1980**, *102*, 951.
(9) Eyring, G.; Schmidtke, H. H. *Ber. Bunsenges. Phys. Chem.* **1981**, *85*, 597.
(10) Heller, E. J. *J. Chem. Phys.* **1975**, *62*, 1544.
(11) Heller, E. J. *Acc. Chem. Res.* **1981**, *14*, 368.
(12) Heller, E. J.; Sundberg, R. L.; Tannor, D. *J. Phys. Chem.* **1982**, *86*, 1822.
(13) Myers, A. B.; Mathies, R. A.; Tannor, D. J.; Heller, E. J. *J. Chem. Phys.* **1982**, *77*, 3857.
(14) Tutt, L.; Tannor, D.; Heller, E. J.; Zink, J. I. *Inorg. Chem.* **1982**, *21*, 3859.
(15) Yoo, C. S.; Zink, J. I. *Inorg. Chem.* **1983**, *22*, 2476.
(16) Tutt, L.; Tannor, D.; Schindler, J.; Heller, E. J.; Zink, J. I. *J. Phys. Chem.* **1983**, *87*, 3017.
(17) Yang, Y. Y.; Zink, J. I. *J. Am. Chem. Soc.* **1984**, *106*, 1500. Yang, Y. Y.; Zink, J. I. *Inorg. Chem.*, submitted for publication.

0002-7863/86/1508-5830$01.50/0

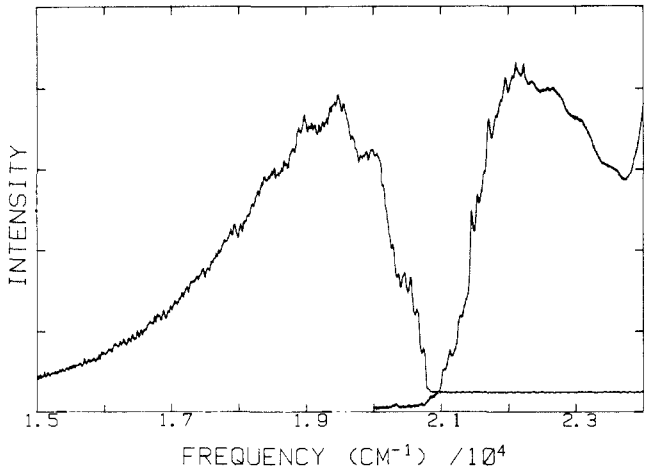

Figure 1. Absorption spectrum (right) and emission spectrum (left) of a single crystal of W(CO)$_5$pyr at 10 K.

and general spectroscopic effect, the "MIME effect", is defined and discussed.[16] The measured bond lengthenings are caused by populating antibonding orbitals in the excited state. The connections between the bond lengthenings and the photochemical reactivity are discussed.

Experimental Section

Electronic Spectra. Electronic absorption spectra of single crystals were taken at 10 K by using the instrument described previously.[18] The single crystals of desired thinness were obtained by growing them between quartz plates from THF in a THF solvent atmosphere. Electronic emission spectra were taken from macroscopic crystals and from powders mounted in a Displex closed-cycle helium refrigerator. The luminescence was excited with the UV lines of an argon ion laser, passed through a Spex 3/4 meter monochrometer, and recorded by using an RCA C31034 photomultiplier, photon-counting equipment, and an LSI 11/02 computer.

Raman Spectra. The Raman spectra were obtained with an argon ion laser as the exciting source. Polycrystalline samples were used. The raman scattering was detected at right angles to the excitation by passing it through a Spex double monochrometer to a C31034 photomultiplier. The spectra were recorded by using photon counting and an LSI 11/02 computer. The spectra were recorded digitally. The intensities were determined by integration via a program that interactively and graphically allows the placement of the base line (which may be sloped) and then integrates the peaks. The experimental uncertainty in the integrations is about 20%.

Crystallography. The X-ray structure was performed on a crystal 0.1 × 0.1 × 0.2 mm. The crystals of W(CO)$_5$pyr (pyr = pyridine) tend to grow from THF as long needles. The diffractometer used was a Syntex, which collected 1848 reflections on the room-temperature crystal. The space group is *Pbam* with $Z = 8$. The tungsten atom and the pyridine ligand are located on the mirror planes. The crystallographic independent unit consists of two half-molecules. The pertinent crystal data are given in the supplementary material. The lorentz polarization and absorption corrections were applied (range 0.96 to 0.94). The structure was solved via the heavy atom method on Fourier maps and difference Fourier maps. Hydrogen atom positions were calculated. Anisotropic thermal parameters were used for all nonhydrogen atoms. Isotropic thermal parameters were fixed at $U_{iso} = 0.0253$ Å^2. All atomic scattering factors and anomalous dispersion corrections were from the *International Tables for X-ray Crystallography* (1974). All calculations were performed on a UCLA Departmental DEC VAX 11/780 using the UCLA Crystallographic Package (locally edited versions of Caress, Orfls, Orffe, Ortep2, Hydrogen). The R factor converged to 0.063.

Theory

The time-dependent theory of molecular spectroscopy provides both a quantitative and an intuitive physical picture of the interrelationship between preresonance Raman spectra and electronic absorption and emission spectra.[11,12] In both types of spectroscopy, the spectra are governed by the motion of a wavepacket on the final multidimensional electronic state potential hypersurface. A cross section of the multidimensional surface along one normal mode, which will be used to discuss the theory, is shown in Figure 2.

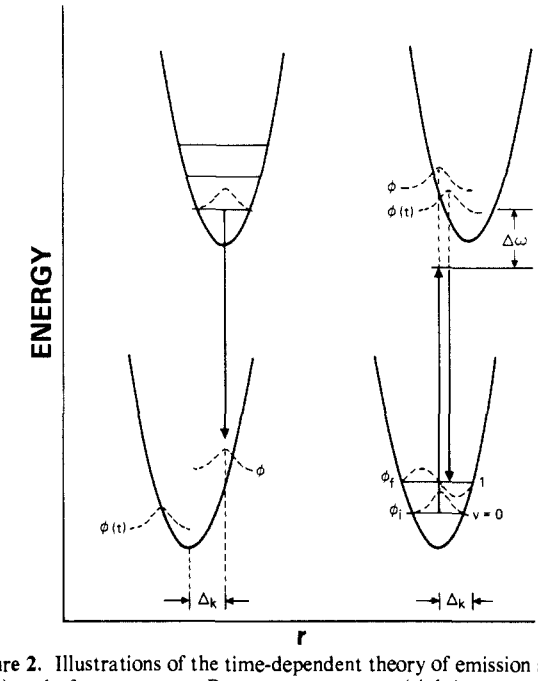

Figure 2. Illustrations of the time-dependent theory of emission spectra (left) and of preresonance Raman spectroscopy (right).

Electronic Absorption and Emission Spectroscopy. The emission process is illustrated on the left side of Figure 2. The initial vibrational wavepacket, ϕ, propagates on the lower potential surface which, in general, is displaced relative to the upper surface. The displaced wavepacket is not a stationary state and evolves according to the time-dependent Schrodinger equation. The quantity of interest is the overlap of the initial wavepacket with the time-dependent wavepacket, $\langle\phi|\phi(t)\rangle$. The overlap is a maximum at $t = 0$ and decreases as the wavepacket moves away from its initial position. At some later time t, the wavepacket may return to its initial position, giving rise to a recurrence of the overlap. A plot of the overlap as a function of time in the time domain shows the initial overlap decreasing and then recurring at a time t when the wavepacket (and thus all of the atoms in the molecule) returns to its original position. This pattern is repetitive. In the simple case of harmonic potential surfaces and no change in vibrational frequencies between the ground and excited electronic states, the overlap is

$$\langle\phi_k|\phi_k(t)\rangle = \exp[-\sum_k(\Delta_k/2(1 - e^{i\omega_k t} - i\omega_k t/2))] \quad (1)$$

where ω_k and Δ_k are the frequency and the displacement of the kth normal mode.

The electronic emission spectrum in the frequency domain is the Fourier transform of the overlap in the time domain. The emission spectrum is then given by

$$I(\omega) = C\omega^3 \int_{-\infty}^{\infty} e^{i\omega t}\langle\phi_k|\phi_k(t)\rangle\, dt \quad (2)$$

where C is a constant, ω is the frequency of emitted radiation, and the other quantities are those defined above. Thus, the emission spectrum can be calculated when the frequencies ω_k and the displacements Δ_k of the normal modes are known.

The time-dependent theoretical treatment of the electronic absorption spectrum is very similar to that of the emission spectrum. The principal difference is that the initial wavepacket starts on the lower (ground state) electronic surface and propagates on the excited electronic state surface. The overlap of the initial wavepacket with the time-dependent wavepacket is given by eq 1. The absorption spectrum is given by

$$I(\omega) = C\omega \int_{-\infty}^{\infty} e^{i\omega t}\langle\phi_k|\phi_k(t)\rangle\, dt \quad (3)$$

(18) Chang, T. H., Zink, J. I. *J. Am. Chem. Soc.* **1984**, *106*, 287.

where all of the symbols are the same as those in eq 2. Note that for absorption, the intensity is proportional to the first power of the frequency times the Fourier transform of the time-dependent overlap.

In most transition metal and organometallic compounds, many normal modes are displaced. The expressions discussed above describe the case where one specific normal mode (the kth) is displaced. In the usual case of many displaced normal modes, the total overlap is given by

$$\langle\phi|\phi(t)\rangle = \prod_k \langle\phi_k|\phi_k(t)\rangle \exp(iE_0t/\hbar - \Gamma^2t^2) \quad (4)$$

where the shift of the electronic energy between the minima of the two surfaces E_0 and a Gaussian damping factor Γ have been included. The complete overlap is thus

$$\langle\phi|\phi(t)\rangle = \exp\{-\sum_k[(\Delta_k^2/2)(1 - e^{-i\omega_kt}) - i\omega_kt/2] - iE_0t/\hbar - \Gamma^2t^2\} \quad (5)$$

This expression for the complete overlap is Fourier transformed to give the electronic absorption or emission spectrum. In order to carry out the calculation it is necessary to know the frequencies ω_k and the displacements Δ_k for all of the displaced normal modes. In addition, the energy difference between the minima of the two potential surfaces E_0 and the damping Γ must be known. As will be discussed below, the frequencies and displacements can be experimentally determined from preresonance Raman spectroscopy, and the energy difference between the ground and excited states and the damping can be obtained from the electronic absorption spectrum and/or emission spectrum.

The damping factor Γ arises because there is relaxation into other modes, the "bath", etc. It is instructive to examine the meaning of the damping factor in the time domain. At one extreme, it will have a value of 0 if every atom in the molecule returns to exactly its starting position at the same time during the time evolution of the system. This condition means that each of the wavepackets in eq 4 must have a recurrence in the overlap at time t which is equal to the overlap at $t = 0$. If even one atom of the molecule does not return to exactly its starting position at that time t, the total overlap in eq 4 will be smaller at time t than at time $t = 0$. The effect of a nonzero damping factor is to decrease the value of the recurrence of the overlaps in the time domain. The effect on the spectrum in the frequency domain is to decrease the resolution, i.e., to "fill in" the spectrum. In the case where the damping is large enough to prevent any recurrence, the spectrum in the frequency domain will consist of only the envelope with no vibronic structure.

Raman Spectroscopy. The time-dependent picture of Raman spectroscopy is shown on the right side of Figure 2. The initial wavepacket propagates on the upper excited electronic state potential surface. However, the quantity of interest is the overlap of the time-dependent wavepacket with the *final* state ϕ_f, i.e., $\langle\phi_f|\phi(t)\rangle$. The Raman scattering amplitude in the frequency domain is the half Fourier transform of the overlap in the time domain,

$$\alpha_{fi}(\omega_i) = \int_0^\infty e^{i\omega_it-\Gamma t}\langle\phi_f|\phi_i(t)\rangle\, dt \quad (6)$$

It is very difficult to experimentally obtain the values of the scattering cross section. However, it is relatively easy to obtain the intensity of a given normal mode k relative to that of another mode k'. A simple expression relating the relative intensities has been derived for the special conditions of harmonic oscillators, no Duschinsky rotation, no change in normal mode frequencies, and preresonance (short time) condition spectra.[12] Under these conditions the relative intensities of two modes is given by

$$\frac{I_k}{I_{k'}} = \frac{\Delta_k^2\omega_k^2}{\Delta_{k'}^2\omega_{k'}^2} \quad (7)$$

The important experimental condition which must be fulfilled is the short time, preresonance condition. When the incident frequency is slightly off resonance with the excited electronic state of interest, the propagation time of the wavepacket on the upper potential surface is governed by the time–energy uncertainty principle $\Delta\omega\Delta t \sim 1$, where $\Delta\omega$ is the frequency mismatch. Under short time conditions the wavepacket moves in a region localized near the equilibrium geometry of the ground electronic state, i.e., the Franck-Condon region. The preresonance Raman intensity is dominated by the slope of the potential surface in this region. The greater the slope, the greater the motion of the wavepacket in Figure 2, the greater the overlap with the final state, and the greater the intensity.

Calculation of Excited-State Distortions and Electronic Spectra from Raman Intensities. The dynamics of the wavepacket on the upper potential surface determines both the absorption spectrum and the Raman spectrum. The emission spectrum is determined by the dynamics on the ground-state potential surface with the same displacements as those which determine the absorption and Raman. In the short time limit, which is valid when the exciting laser line is just below E_{00} and/or there are many displaced modes in the molecule, the intensities in the Raman spectrum are related to the displacements by eq 7. In the short time limit, the absorption spectrum becomes

$$I(\omega) = C\omega \exp[-(\omega - E)^2/2\sigma^2] \quad (8)$$

The quantity $2\sigma^2$ is the width of the electronic absorption spectrum at $1/e$ of the height. This quantity is also related to the displacements

$$2\sigma^2 = \sum\Delta_k^2\omega_k^2 \quad (9)$$

Thus $2\sigma^2$ is experimentally found from the absorption spectrum, ratios of the Δ's are found from the Raman spectrum, and the Δ_k's are calculated (except for sign) by pairwise comparison of the Raman intensities. Once the Δ_k's are calculated, the emission spectrum is calculated by using eq 2.

The two major sources of error in the calculations on real molecules stem from the approximations listed above. First, the derivation assumes that only one state, the emitting state, contributes to the preresonance Raman intensities. In large molecules, other nearby excited states could also contribute to the intensities. An excitation profile can be used to evaluate the validity of the above assumption. However, both the high photochemical quantum yields and luminescence of the organometallics studied here have prevented good quality excitation profiles from being obtained. Second, eq 7 was derived by assuming that the ground- and excited-state vibrational frequencies are equal. In general, the frequencies will be different. In this case eq 7 becomes

$$\frac{I_k}{I_{k'}} = \frac{f_{k'}^4}{f_k^4}\frac{\omega_k^2}{\omega_{k'}^2}\frac{\Delta_k^2}{\Delta_{k'}^2} \quad (10)$$

where $f_k = \omega_{k,\text{ground}}/\omega_{k,\text{excited}}$. Usually the excited-state vibrational frequencies are not known and eq 10 cannot be used. The magnitude of the error in the relative distortions calculated by using eq 7 neglecting the frequency change depends on the ratios of the f's for the two modes being compared.

Results

1. Emission Spectra. The emission spectrum of a single crystal of $W(CO)_5$pyr taken at 10 K is shown in Figure 3. The emission has been assigned to the $^3E \rightarrow {}^1A_1$, d_{z^2} to (d_{xz},d_{yz}) transition.[19-23] The spectrum shows two types of resolved structure: a low-frequency progression with a peak-to-peak separation of 90 cm^{-1}, and a long regularly spaced progression with a peak-to-peak separation of 550 ± 10 cm^{-1}. The emission spectrum of $W(CO)_5$pyr in a 2-MeTHF glass at 10 K showed the 550-cm^{-1} progression but did not contain the 90-cm^{-1} peaks. Thus the

(19) Wrighton, M. S.; Hammond, G. S.; Gray, H. B. *J. Am. Chem. Soc.* **1971**, *93*, 4336.
(20) Wrighton, M. S.; Abrahamson, H. B.; Morse, D. L. *J. Am. Chem. Soc.* **1976**, *98*, 4105.
(21) Dahlgren, R. M.; Zink, J. I. *Inorg. Chem.* **1977**, *16*, 3154.
(22) Dahlgren, R. M. *Ph.*D. Thesis, University of California, Los Angeles, 1978.
(23) Boxhoorn, G.; Oskam, A.; Gibson, E. P.; Narayanaswamy, R.; Rest, A. J. *Inorg. Chem.* **1981**, *20*, 783.

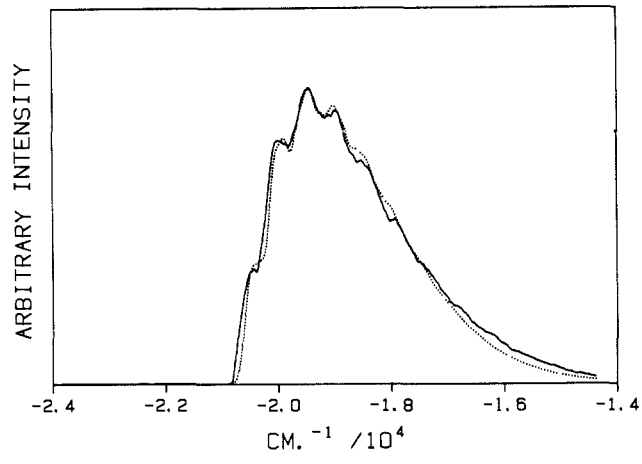

Figure 3. Experimental (solid line) and calculated (dotted line) emission spectra of W(CO)$_5$pyr. The calculated spectrum was obtained by using exactly the preresonance Raman determined distortions given in Table I; E_0 = 20 500 cm^{-1}, and Γ = 72 cm^{-1}. The sharp phonon structure in the experimental spectrum was smoothed to facilitate comparison of the broad features.

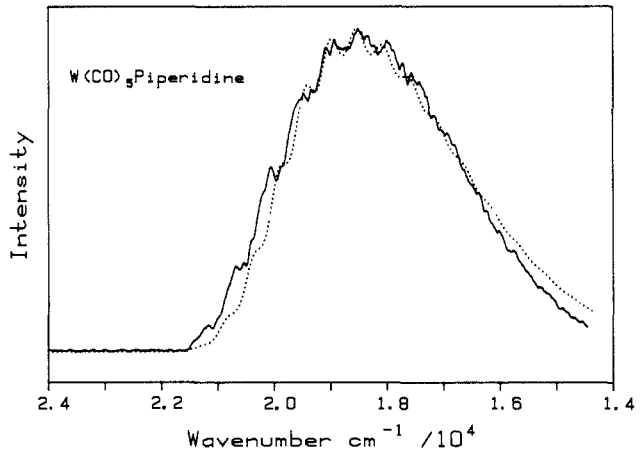

Figure 4. Experimental (solid line) and calculated (dotted line) emission spectra of W(CO)$_5$piperidine. The calculated spectrum was obtained by using the preresonance Raman determined distortions given in Table I; E_0 = 21 258 cm^{-1}, and Γ = 113 cm^{-1}.

90-cm^{-1} peaks are tentatively assigned to a crystal lattice mode. The most unusual aspect of the spectra is the 550-cm^{-1} progression. In a luminescence spectrum, a regularly spaced progression is almost always caused by distortion along a totally symmetric normal mode. Its frequency is equal to the vibrational frequency of that mode in the ground electronic state. Surprisingly, there are no totally symmetric normal modes with a frequency of 550 cm^{-1} (vide infra).

The emission spectrum of a single crystal of W(CO)$_5$pip (pip = piperidine) is shown in Figure 4. The emission is assigned to the $^3E \rightarrow {}^1A_1$, d_{z^2} to (d_{xz},d_{yz}) transition. Two progressions are again observed. The smaller progression with a peak-to-peak separation of 80 cm^{-1} is again attributed to a crystal lattice mode for the same reasons as above. The second progression is a long, regularly spaced progression with a peak separation of 520 ± 15 cm^{-1}. The major difference this spectrum and that of the pyridine complex is that the progression is significantly longer. The peak maximum occurs at the sixth vibrational quantum instead of the third. This progression is also unusual because there is no ground-state normal vibrational mode with an energy near 520 cm^{-1} (vide infra).

2. Absorption Spectrum of W(CO)$_5$pyr at 10 K. The single crystal polarized electronic absorption spectrum of the low-energy region of W(CO)$_5$pyr is shown in Figure 1. This band, with a maximum at 22 100 cm^{-1}, has been well characterized from solution absorption spectra.[19-22] In the spectrum shown in Figure 1, the polarizer was adjusted such that the band to higher energy is forbidden and the band for the transition from the ground state to the lowest energy excited states, ^3E, is measurable. In the orthogonal polarization direction, the total absorbance of all peaks except the first four phonon peaks and the first of the 520-cm^{-1} vibronic peaks was too large to be recorded. Even in the most favorable polarization condition which was obtained, the lowest energy peak is overlapped on its high-energy side by an intense transition. Despite the overlap, the low-frequency phonon mode and the higher frequency progression are observed.

Table I. Preresonance Raman Intensities and Calculated Distortions

ω_k/(cm^{-1})	I_k/I_{636}[a]	Δ_k/Δ_{636}[b]	emission best fit[c]
W(CO)$_5$(pyridine)			
2075	1.82 (0.51)	0.28 (0.04)	0.28
1973	1.27 (0.36)	0.24 (0.03)	0.24
1953	0.46 (0.13)	0.15 (0.02)	0.15
1934	0.38 (0.11)	0.14 (0.02)	0.14
1890	1.36 (0.38)	0.27 (0.04)	0.27
1651	0.47 (0.13)	0.18 (0.03)	0.18
1607	2.18 (0.61)	0.39 (0.05)	0.39
1489	0.10 (0.03)	0.10 (0.01)	0.10
1223	1.45 (0.41)	0.43 (0.06)	0.43
1073	0 83 (0.23)	0.37 (0.05)	0.37
1012	3.59 (1.01)	0.81 (0.11)	0.81
636	1.00 (0.28)	0.68 (0.10)	0.68
602	0.79 (0.22)	0.64 (0.09)	0.64
470	0.38 (0.11)	0.56 (0.08)	0.56
462	0.86 (0.24)	0.87 (0.12)	0.87
434	1.17 (0.32)	1.08 (0.15)	1.08
427	1.00 (0.28)	1.01 (0.14)	1.01
195	0.41 (0.12)	1.42 (0.20)	1.42
W(CO)$_5$ (piperidine)			
ω_k (cm^{-1})	I_k/I_{484}[a]	Δ_k/Δ_{484}[b]	emission best fit$_c$
2950	(0.21)	0.13	0.14
2930	(0.26)	0.14	0.16
2069	(0.94)	0.39	0.43
1982	(0.56)	0.32	0.36
1970	(1.71)	0.56	0.61
1919	(0.35)	0.27	0.31
1905	(0.40)	0.29	0.32
1860	(1.09)	0.49	0.54
1837	(0.83)	0.43	0.49
1030	(0.05)	0.20	0.22
810	(0.10)	0.34	0.38
596	(0.14)	0.54	0.79
484	(1.00)	1.78	2.38
433	(0.82)	1.80	1.80
426	(0.60)	1.57	1.54
414	(0.90)	1.96	1.58
377	(0.05)	0.49	0.54
256	(0.08)	0.93	0.85

[a] The experimental uncertainties are 20% of the vlaue unless otherwise shown. [b] The relative displacements are given for the dimensionless normal coordinates and are scaled to the total distortion. [c] The values of the relative displacements which were used to calculate the experimental luminescence spectra shown in Figures 3 and 4. In the case of W(CO)$_5$pyr, exactly the experimental values were used.

3. Raman Spectra. The preresonance Raman data for W(CO)$_5$pyr and W(CO)$_5$pip are given in Table I. The 476.5-nm argon ion laser line was used to obtain the preresonance Raman spectrum of W(CO)$_5$pyr, and the 488-nm line was used to obtain the spectrum of W(CO)$_5$pip. The relative intensities of the peaks were determined by integrating the peaks. All of the peaks in the experimental spectrum having intensities greater than 3% of that of the most intense peak were measured and used in the calculations. The photosensitivity and luminescence of the compounds prevented usable excitation profiles from being obtained. The major effect on the relative distortions caused by moving the exciting laser line away from the absorption band is an increase in the relative distortion of the 195-cm^{-1} normal mode. The spectrum obtained by exciting at 476.5 nm was used in the calculations discussed below because its energy (20 986 cm^{-1}) places

Table II. Bond Lengths in the Ground Electronic State

bond	length (Å)
W–C (axial)	2.00 ± 0.01
W–C (equatorial)	2.04 ± 0.02
W–N	2.26 ± 0.01
C–O (axial)	1.13 ± 0.01
C–O (equatorial)	1.12 ± 0.02

it almost perfertly in preresonance with the lowest energy absorption band (cf. Figure 1).

4. Ground-State Structure of $W(CO)_5$pyr. The structure of the molecule of interest in its ground electronic state must be known in order to calculate the structure in the excited electronic state. The time-dependent theory provides a method of calculating the *distortions* of the molecule along various normal modes, i.e., of calculating the *changes* in bond lengths and angles. Thus the ground-state bond lengths and angles must be known in order to determine the excited-state structure.

A second motivation for obtaining the crystal structure was to determine the molecular packing in order to interpret the single crystal absorption spectrum. Unfortunately the molecules pack in such a manner that the molecular x and z axes are mixed in the crystal spectrum and pure x or z polarized spectra cannot be obtained. The structural aspects of the polarized absorption spectrum were not pursued further.

The crystal structure shows that there are two symmetry-independent molecules per unit cell. The atomic positions of the atoms are given in the supplementary material. The z axes of the molecules (i.e., the W–N bond directions) are not parallel. However, they lie in a plane mixed with the x axis (i.e., the axis parallel to the pyridine ring's plane). The y axes are perpendicular to the pyridine ring's plane and are all parallel to the c axis. The symmetry of an individual molecule is C_{2v}. The site symmetry is C_s.

Selected bond lengths, which will later be compared to bond-length changes in the excited state, are given in Table II. The length of the carbon–tungsten bond trans to the pyridine ligand is 2.00 Å, slightly shorter than the cis W–C bond lengths. The cis W–C bond lengths are 2.04 Å. The W-N bond length is 2.27 Å. The plane of the pyridine ring almost bisects the equatorial C–W–C bond. All ligand–metal–ligand bond angles are within 0.7° of 90°.

5. Calculation of the Emission Spectra of $W(CO)_5$pyr from Raman Intensities. The combination of experimental electronic spectra and Raman spectra in conjunction with time-dependent theory provides a powerful method for quantitatively calculating the distortions and spectra and for interpreting the detailed information about excited electronic states contained in the data. The electronic spectrum is calculated by using eq 2 and 5. The distortions used in these equations are determined from the preresonance Raman intensities given in Table I by using eq 7 and 9.

Both the vibrational frequencies of the normal modes and the displacements of the excited-state potential surfaces along these normal modes are obtained from the preresonance Raman spectrum. The intensity of a Raman peak at a given frequency is related to the slope of the excited-state potential surface along that normal mode. The greater the slope, the greater the displacement, the greater the motion of the wavepacket, the greater the overlap, and thus the greater the Raman intensity.

Once the relative displacements of the excited-state surface along the normal modes are determined, the wavepacket is propagated on the multidimensional hypersurface, and the overlap $\langle\phi|\phi(t)\rangle$ is calculated from eq 5. The overlap in the time domain is then Fourier transformed (eq 2) to give the calculated electronic spectrum in the frequency domain. When good agreement between the calculated electronic spectrum and the experimentally determined spectrum is found, the agreement indicates that the simplifying assumptions discussed previously are met and that the distortions which are calculated are meaningful.

The emission spectrum of $W(CO)_5$pyr calculated as discussed above is shown in Figure 3. In this calculation, *exactly* the displacements and frequencies described from the experimental Raman data given in Table I were used. Excellent agreement between the experimental spectrum and the theoretical spectrum calculated from the 18-dimensional excited-state potential surface is obtained. Interpretation of these results will be discussed below.

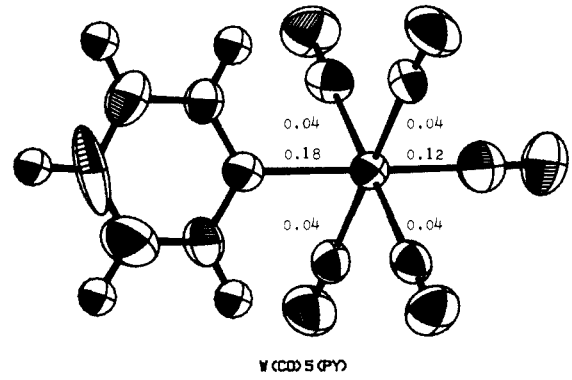

Figure 5. Changes in the bond lengths (in angstroms) of $W(CO)_5$pyr in its lowest excited electronic state.

6. Calculation of the Emission Spectrum of $W(CO)_5$pip from Raman Intensities. The emission spectrum of $W(CO)_5$pip was calculated in the manner described above. The calculated spectrum is shown superimposed on the experimentally determined spectrum in Figure 4.

The agreement between the calculated and experimental spectra is not as good as that in Figure 3. Two factors are probably involved. First, the excited state is significantly more distorted than that in $W(CO)_5$pyr. Thus more vibrational quanta are involved and anharmonicity, which was not included in the calculation, will play a larger role. Secondly, the W–N stretching mode was not observed in the Raman spectrum. It is probably at lower energy than the W–N stretch in the pyridine complex. Even if a low-frequency mode has a significant distortion, the observed relative intensity will be small because of the inverse frequency squared term in eq 7. The major effect of a very low frequency mode on the emission spectrum can be included in the damping factor (vide infra). These considerations explain why a larger damping factor is required for piperidine than for pyridine.

7. Excited-State Distortions and Structures. The excited-state geometries of the $W(CO)_5$pyr and $W(CO)_5$pip complexes in their lowest excited electronic states are calculated by converting the relative displacements, given in Table I, to bond length changes in angstrom units. First, the relative displacements are converted to absolute displacements by using eq 7 and 9. The value of $2\sigma^2$ is obtained from the emission spectrum. The resulting displacements, Δ_k, are converted from dimensionless normal coordinates to lengths and angles by transforming to the desired units. A complete calculation requires a complete normal coordinate analysis. A good approximation is achieved by assuming that the normal coordinates are uncoupled and that the masses appropriate to a specific normal coordinate can be used. The latter calculation is reported here because a complete normal coordinate analysis is not available for the molecules studied in this paper.

The calculated changes in the bond lengths (in Å) for $W(CO)_5$pyr are shown in Figure 5. The most highly elongated bond is the W–N bond. The W–C bond trans to the pyridine is also highly elongated. The lengths of the W–C bonds cis to the pyridine are only slightly changed. The excited-state bond lengths (Å) are W–N, 2.44, trans W–C, 2.12, and cis W–C, 2.08. All of the WCO bond angles of the carbonyls cis to the pyridine are changed from 180°. A determination of the angle change in degrees requires a normal coordinate analysis. The meaning of the bond length changes in terms of the bonding changes in the excited state and the connections of these bond lengthenings to the photochemical reactivity of the molecule are discussed below.

The bond length changes in the $W(CO)_5$pip complex are larger than those in the pyridine complex. The W–C bond trans to the piperidine is lengthened by 0.25 Å and the cis W–C bonds are lengthened by 0.05 Å. The bond length change of the W–N bond

has an upper limit of 0.3 Å. The photochemical implications are discussed below.

Discussion

1. Orbital Characteristics of the Lowest Excited State. The lowest energy excited state of C_{4v} W(CO)$_5$L compounds (where L is a ligand lower in ligand field strength than CO) has been assigned by Wrighton et al. to the (d_{xz},d_{yz}) to d_{z^2} transition.[19,20] This assignment has been confirmed by detailed spectroscopic studies including MCD spectroscopy.[24-26] Both the pyridine and piperidine complexes have ^{3}E lowest energy excited states.

The orbital components of the lowest energy excited state in C_{4v} d^6 complexes are given by eq 11.[27] Because of the proximity

$$\phi E = \frac{1}{\sqrt{1+\lambda^2}}\left[\frac{\sqrt{3}+\lambda}{2}(d_{xy}^2 d_{xz}^2 d_{yz}^1 d_{z^2}^1) + \frac{1-\sqrt{3}\lambda}{2}(d_{xy}^2 d_{xz}^2 d_{yz}^1 d_{x^2-y^2}^1)\right] \quad (11)$$

of other states of the same symmetry, mixing occurs and both d_{z^2} and $d_{x^2-y^2}$ orbital character is involved. The mixing coefficient λ is related to the difference between the ligand field strengths of the carbonyl ligand and the unique ligand.[27] For an octahedron (where L = CO), $\lambda = 0$, and the σ interactions between the metal and all six ligands are equal. When the unique ligand L is weaker than carbonyl as is the case for pyridine and piperidine, $\lambda > 0$, and the increase in d_{z^2} character over $d_{x^2-y^2}$ character causes increased σ antibonding in the z direction compared to that in the xy plane. The relationship between λ and the percent d_{z^2} character has been discussed in detail.[28] The most important conclusions from these orbital considerations are that (1) in the one-electron ligand field orbital picture of W(CO)$_5$pyr and W(CO)$_5$pip, the d_{z^2} orbital lies lower in energy than the $d_{x^2-y^2}$ orbital; and (2) the lowest energy excited state wave function is dominated by a large d_{z^2} character.

The excited-state distortions can be qualitatively predicted from the orbital characteristics.[28] The d_{z^2} orbital and the $d_{x^2-y^2}$ orbital are both σ antibonding molecular orbitals. Populating the d_{z^2} orbital is thus expected to weaken σ bonding primarily in the z direction. Populating the $d_{x^2-y^2}$ orbital is expected to weaken σ bonding in the xy plane. The larger the value of λ in eq 10, the greater the bond weakening in the z direction.[28]

The largest distortion expected for W(CO)$_5$pyr and W(CO)$_5$pip, based on the above considerations, is metal–ligand bonding lengthening along the z axis, the axis containing the unique ligand. Smaller but nonzero distortions are also to be expected in the xy plane. Although metal–ligand bond lengthenings are predicted to be the biggest distortions, small changes in bond lengths in the ligands themselves are also expected. For example, lengthening a W–CO bond should reduce back-bonding to the CO, thus strengthening the CO bond and decreasing the CO bond length. Small changes are also expected in the pyridine ring.

Trends in the magnitudes of the major distortions can also be predicted from eq 11. The piperidine ligand is a weaker ligand in the spectrochemical series than pyridine. (The energy of the absorption maximum is 22 100 cm^{-1} in W(CO)$_5$pip and 22 400 cm^{-1} in W(CO)$_5$pyr.) Thus λ is larger for the piperidine complex than that for the pyridine complex, and the distortions along the z axis should be greater.

The experimental results provide the first spectroscopic substantiation of the ligand field based bonding predictions. The largest experimentally determined distortions occur along the z axis and smaller distortions occur in the xy plane. The piperidine complex is more highly distorted than the pyridine complex. Small distortions of the bond lengths within the ligands are also observed. The predicted bonding changes which have been used to predict photochemical reactivity are verified by the combination of preresonance Raman spectroscopy, electronic spectroscopy, the time-dependent theory.

2. Correlations between Excited-State Distortions and Photochemical Reactivity. The ligand field theory of transition metal photochemistry is based on the idea that the bonding changes in excited electronic states are correlated with ligand photolabilization.[29-31] Populating the d_{z^2} or $d_{x^2-y^2}$ orbitals increases σ antibonding in the z and xy directions, respectively. Depopulating d orbitals which have π symmetry simultaneously change the π bond order with a directionality determined by which d orbital is depopulated. σ and π bond weakening along a given metal–ligand bond is correlated with the photochemical ligand labilization of that bond.

In cases such as those studied here where two different ligands are on the same molecular axis such as the z axis, the more complicated question arises of which of the two ligands experiences the greatest antibonding. Three approaches to answering this question have been used. The first successful approach used molecular orbital theory, specifically overlap populations, to calculate the distribution of antibonding along a given axis.[32] This approach is predictive, but it requires a complete calculation for each compound of interest. A second approach uses ligand field theory. When the original theory is rewritten in terms of angular overlap parameters, contributions from each ligand can be apportioned.[31] This approach is also predictive, but it is not useful for many metals because the required parameters have not or cannot be determined. The third approach, used specifically for tungsten carbonyls, is an empirical analysis based on infrared data.[21] It is to some extent predictive for compounds far from the empirical dividing lines. The above three approaches are indirect methods of inferring antibonding character in a given excited state.

The bond length changes determined from preresonance Raman spectra, electronic spectra, and time-dependent theory provide a detailed picture of the results of bonding changes caused by populating excited electronic states. There is a direct but not linear correlation between bond length changes and the photochemical labilizations of the ligands. In the pyridine complex, the most highly distorted metal–ligand bond, the W–N bond, is lengthened by 0.18 Å. The quantum yield for pyridine loss is 0.22. The much less distorted metal–carbon bond is much less reactive; the quantum yield for CO loss is less than 0.01. It is interesting to note that the piperidine complex has a larger distortion and a larger quantum yield for unique ligand loss, 0.58, than the pyridine complex. Further work is needed to determine whether or not this type of correlation is general for W(CO)$_5$L complexes.

3. The Missing Mode Effect (MIME). Both of the compounds W(CO)$_5$pyr and W(CO)$_5$pip exhibit the "missing mode effect" (MIME), a regularly spaced vibronic progression in the luminescence spectrum which does not correspond to any ground-state normal mode vibration.[16] In the luminescence spectrum of W(CO)$_5$pyr, the MIME spacing is 550 cm^{-1}, and in the luminescence spectrum of W(CO)$_5$pip the MIME spacing is 520 cm^{-1}. No totally symmetric vibrational modes of the frequencies are found in the vibrational spectra of these molecules.[33-35]

The MIME effect is easily understood from the viewpoint of time-dependent theory. In the time domain, the most important characteristics of the overlap are the rapid decrease near $t = 0$, the partial recurrence in the overlap near $t_m = 2\pi/\omega_m$ (where ω_m is the frequency spacing of the observed progression in the fre-

(24) Schreiner, A. F.; Amer, S.; Duncan, W. M.; Ober, G.; Dahlgren, R. M.; Zink, J. I. *J. Am. Chem. Soc.* **1980**, *102*, 6871.
(25) Wallin, S. A.; Schreiner, A. F. *Inorg. Chem.* **1983**, *22*, 1964.
(26) Boxhoorn, G.; Stufkens, D. J.; van de Coolwijk, P. J. M.; Hezemans, A. M. F. *Inorg. Chem.* **1981**, *20*, 2778.
(27) Incorvia, M. J.; Zink, J. I. *Inorg. Chem.* **1974**, *13*, 2489.
(28) Zink, J. I. *Inorg. Chem.* **1973**, *12*, 1018.
(29) Zink, J. I. *J. Am. Chem. Soc.* **1972**, *94*, 8039.
(30) Wrighton, M.; Gray, H. B.; Hammond, G. J. *Mol. Photochem.* **1973**, *5*, 165.
(31) Van Quickenbourne, H. G.; Ceulemans, A. J. *J. Am. Chem. Soc.* **1977**, *99*, 2208.
(32) Zink, J. I. *J. Am. Chem. Soc.* **1974**, *96*, 4464.
(33) Brown, R. A.; Dobson, G. R. *Inorg. Chim. Acta* **1972**, *6*, 65.
(34) English, A. M.; Plowman, K. R.; Butler, I. S. *Inorg. Chem.* **1981**, *20*, 2553.
(35) Dillinger, R.; Gliemann, G. *Chem. Phys. Lett.* **1985**, *122*, 66.

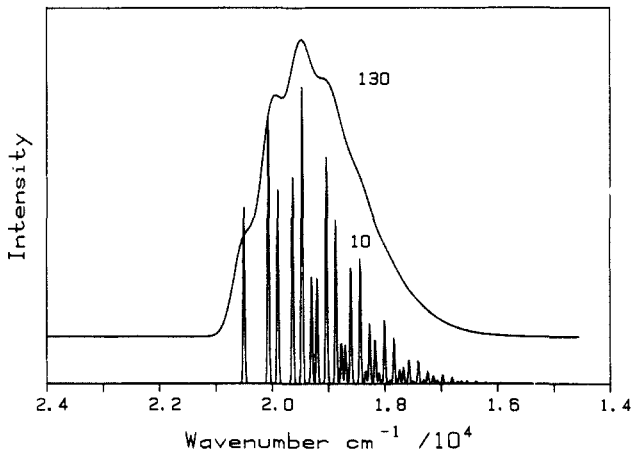

Figure 6. The effect of Γ, the damping factor, on the electronic spectrum. The example shown here contains two distorted normal modes with frequencies ω_1 = 430 cm^{-1} and ω_2 = 600 cm^{-1}. When Γ is small (Γ = 10 cm^{-1}), the spectrum is highly resolved, and the individual vibronic peaks are clearly seen. A large value of Γ (Γ = 130 cm^{-1}) fills in the spectrum.

quency domain), and the quenching of further recurrences in the time domain due to the damping factor Γ and to the presence of displacements in several different modes. The partial recurrence at $t = t_m$ is responsible for the appearance of the regularly spaced progression at frequency $\omega_m = 2\pi/t_m$. Two or more displaced modes can conspire to give such a partial recurrence which is not expected of any mode alone. In the simplest pedagogical example, a two-mode case, the total overlap is

$$\langle\phi|\phi(t)\rangle = \langle\phi_1|\phi_1(t)\rangle\langle\phi_2|\phi_2(t)\rangle \exp(-iE_0t/\hbar - \Gamma^2t^2) \qquad (12)$$

If $\langle\phi_1|\phi_1(t)\rangle$ and $\langle\phi_2|\phi_2(t)\rangle$ peak at different times, the product $\langle\phi|\phi(t)\rangle$ may peak at some intermediate time. The compromise recurrence time t_m is not just the average of t_1 and t_2. The MIME frequency may be smaller than any of the individual frequencies, but it is usually between the highest and lowest frequencies. It cannot be larger than the highest frequency.

Each of the displaced modes in the molecule can contribute to the MIME frequency. Each of these modes k has a time dependence whose magnitude is given by eq 1. The larger the displacement Δ_k in the kth mode, the sharper the peaks in $\langle\phi_k|\phi(t)\rangle$. The total overlap $\langle\phi|\phi(t)\rangle$ is the product (eq 4) of the individual modes' overlaps, and t_m will have the tendency to be closest to $t_k = 2\pi/\omega_k$ for that mode with the largest Δ_k.

In a series of molecules, the Δ_k's change relative to each other, and the value of t_m (and thus ω_m) can be tuned over large ranges. The MIME frequency need not bear any simple or integer relationship to the normal mode frequencies.

A second key requirement for the MIME effect is that the spectrum must not be fully resolved; i.e., the damping factor Γ must be large. The effect of Γ on the spectrum in the frequency domain is illustrated in Figure 6 for the pedagogical example of two displaced modes. If the damping is small, for example, Γ = 10 cm^{-1}, there will be many recurrences of the overlap (eq 12) in the time domain, and the emission spectrum will exhibit sharp, well-resolved lines as shown at the bottom of the figure. If the damping is increased to 130 cm^{-1}, for example, the recurrences at long times will be damped out and disappear giving a spectrum which is less fully resolved as shown at the top of Figure 6. When the damping is extremely large, there will be no recurrences of the overlap in the time domain and the emission spectrum will consist only of a broad envelope. In the extreme of small damping, no MIME frequency will be observed. Instead, progressions in each of the normal modes and combination bands will be observed. In the case of intermediate damping, the MIME effect can occur. Each vibronic peak in the emission spectrum consists of various contributions from the normal modes and their combinations. Even in the ultrasimple example shown in Figure 6, no simple relationship between an observed vibronic peak and the normal modes contributing to it is apparent. For example, the major contributors to the fourth peak in the poorly resolved spectrum are two unequally weighted combination bands (major contributor, two quanta of the 430-cm^{-1} mode and one quantum of the 600-cm^{-1} mode; minor contributor, one quantum of the 430-cm^{-1} mode and two quanta of the 600-cm^{-1} mode). In the cases of the $W(CO)_5L$ compounds where 18 modes contribute, the situation is too complex to provide a meaningful analysis in the frequency domain.

The 550-cm^{-1} MIME frequency of $W(CO)_5$pyr was calculated by using the Raman-determined distortions and frequencies as described in the theory and results sections above. The normal modes which give a recurrence in the time domain at $t = t_m$ (i.e., a MIME frequency $\omega_m = 2\pi/t_m$ = 550 cm^{-1}) are predominantly the W–C stretches in the 400–500-cm^{-1} region, the WCO bend at 636 cm^{-1}, and the W–N stretch at 195 cm^{-1}. Although all of the modes including the high-frequency CO stretching modes contribute to the MIME frequency, the primary effect on the luminescence spectrum of these modes with small displacements is to "fill in" the red end of the spectrum.

The 520-cm^{-1} MIME frequency of $W(CO)_5$pip was calculated by using the same procedures as those used for $W(CO)_5$pyr. The major contributing modes to the MIME frequency are the W–C stretches in the 400–500-cm^{-1} region and the WCO bending mode at 596 cm^{-1}.

The emission spectra of $W(CO)_5$pyr and $W(CO)_5$pip are typical of the spectra obtained from perturbed polyatomic molecules. The spectra show structure on a scale of 500 wavenumbers although the instrumental resolution is two orders of magnitude higher. The natural tendency to interpret the regular spaced progression in terms of one displaced mode is far from correct. Instead, 18 displaced modes contribute to the observed MIME progression. The origin of the MIME effect is readily explained by using time-dependent theory. In addition, the magnitudes of the displacements of all of the displaced normal modes are determined.

Acknowledgment. The support of the National Science Foundation and the US Army Research Office are gratefully acknowledged. We also thank Professor E. Heller for many stimulating discussions.

Supplementary Material Available: Crystallographic data for $W(CO)_5$pyr (3 pages). Ordering information is given on any current masthead page.